Int J Adv Manuf Technol (2013) 64:1–12
DOI 10.1007/s00170-012-4372-0

ORIGINAL ARTICLE

Study on the basic characteristics of a vortex bearing element

Xin Li · Mikio Horie · Toshiharu Kagawa

Received: 14 June 2011 / Accepted: 3 July 2012 / Published online: 14 August 2012

Abstract A new air bearing element called as vortex bearing is introduced and investigated in this study. In comparison to the conventional orifice bearing, the new bearing is characterized by blowing air through tangential nozzles to form a vortex flow. The study focuses on one vortex-bearing element to investigate its basic characteristics (flow rate characteristics, pressure and velocity distributions, load capacity, and static stiffness). We show that the vortex bearing uses vortex flow to form a sunken negative pressure distribution at the central area, so that it can narrow the gap clearance between the workpiece and the bearing and thereby improve the flotation stiffness. Moreover, blowing air tangentially instead of emitting onto the workpiece directly can avoid the formation of intense pressure distribution on the workpiece's surface, which would reduce the partial stress concentration acting on the workpiece. For these reasons, the new vortex bearing is applicable in air conveyors that float and transport workpieces such as glass substrates and silicon wafers.

Keywords Vortex bearing · Vortex flow · Air conveyor · Flotation stiffness · Bearing force

Nomenclature

d	Diameter of tangential nozzle
D_1	Diameter of vortex chamber
D_2	Outer diameter of the test bearing
F	Bearing force
h	Clearance between the test bearing and the workpiece
H	Height of the vortex chamber
P	Pressure
P_s	Supply pressure
Q	Supply flow rate
r	Position of radial direction
u_α	Tangential velocity
ρ	Density of air

X. Li (✉) · M. Horie · T. Kagawa
Precision and Intelligence Laboratory,
Tokyo Institute of Technology,
R2-14, 4259 Nagatsuta-chou, Midori-ku,
Yokohama 226-8503, Japan
e-mail: li.x.ad@m.titech.ac.jp

1 Introduction

Air conveyors are often used in position and motion control systems because they can remove the effect of friction [1, 2]. Meanwhile, as shown in Fig. 1, air conveyors are also widely used in IC manufacture lines where fragile workpieces such as silicon wafers and large-scale glass substrates of thin flat panels (TFPs) are produced. Transporting using air as the medium can avoid scratching the workpieces; moreover, air does not produce magnetic fields and heat, and therefore, the workpiece itself and peripheral electronic devices will not be affected. We can find many applications and research reports on air conveyors in IC manufacture. In early days, Paivanas and Hassan developed an air conveyor for levitating and moving small-sized silicon wafers (diameter, 57–82 mm) [3]. As the IC manufacturing technology advanced, the size of workpieces increased rapidly. Taking a typical example, a tenth generation TFP glass substrate is nearly 3 m long and 3 m wide. For conveying such large and fragile workpieces safely, the air conveyor plays a role of increasing importance. Several manufacturers have developed large-scale air conveyors to handle the TFP glass substrate [4–7]. Concerning

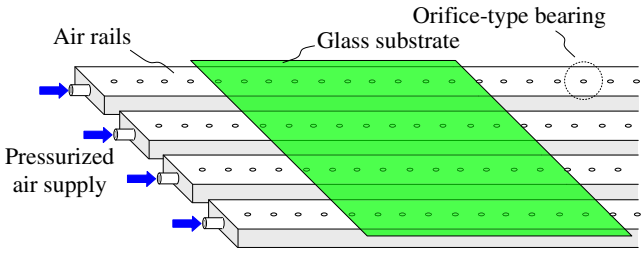

Fig. 1 Air conveyor for floating and transporting glass substrate

research on air conveyors, Srinivas used a finite element method (FEM) to investigate the pressure distribution between the workpiece and the air conveyor [8], and Lee developed some design principles for reducing the equipment cost and air consumption [9], while Amano focused on improving the flotation precision of glass substrate [10].

From the above research reports and actual applications, it is found that most current air conveyors use orifice bearing elements which spout pressurized air from a small hole to float the workpiece (see Fig. 2a). The orifice bearing is one type of external pressurized bearing element [11, 12]. Because air is directly ejected with high speed onto the workpiece and then changes direction to flow into the gap clearance, it will cause a pressure peak and intense pressure drop at the centre, exposing the workpiece to the resulting partial stress concentration [13]. For reducing the partial stress concentration, the orifice bearing element is replaced by a porous material bearing element to avoid excessively distributed pressure [6, 9]. However, it is difficult to ensure that every piece of porous material produced by high-temperature sintering has the same flow characteristics, and the high production cost makes its application difficult in large-scale glass substrate manufacturing lines which require a large quantity of porous material elements. Furthermore, another disadvantage of the orifice bearing element is that it floats the workpiece in a position rather far above the air conveyor, that is, the clearance between the workpiece and the air conveyor is relatively large [13]. This leads to low flotation stiffness and a deficient damping effect against some disturbance from, for example, the down flow in the clean room. Producing a pocket space at the outlet of the orifice can improve the stiffness [14]. However, it is also well known that the pocket space would cause an unstable phenomenon called as a pneumatic hammer [15, 16]. Another way to increase stiffness is to set the supply pressure higher [17, 18]. However, a higher supply pressure would lead to higher air consumption and running cost.

Owing to the above technical problems, Devitt has pointed out that an air conveyor composed merely of an orifice bearing element hardly meets the requirements of the current IC manufacture. Adding vacuum suction ports to the air conveyor is a feasible approach to increase the workpiece's flotation stiffness (see Fig. 2b) [4, 13]. A vacuum suction port is connected to the vacuum generators (vacuum pump or ejector) to drag the workpiece closer to the conveyors, that is, to narrow the clearance between the workpiece and the air conveyor so that higher stiffness and a significant damping effect could be acquired. However, this method needs at least one vacuum generator. Moreover, the positive pressure circuit for flotation and the negative pressure circuit for suction have to be generated simultaneously in the air conveyor, which seriously increases the difficulties of designing and manufacturing air conveyors.

2 Mechanism of vortex bearing

For solving the above problems, a new air-bearing element called as vortex bearing (see Fig. 3) is proposed and tested [7, 19, 20]. It comprises a circular vortex chamber at the centre which has tangential nozzles inserted at both sides and is surrounded by an annular flat skirt. Blue arrow lines show the air flow. Pressurized air is blown through the tangential nozzles into the vortex chamber; it then advances along the circular wall to form the vortex flow. Finally, the air is discharged to the atmosphere by flowing into and through the gap between the annular skirt and the workpiece. Compared to the conventional orifice bearing, this design has two remarkable advantages: (1) the air emitting from the tangential nozzles avoids directly impacting the workpiece, and the air with a tangential velocity component can smoothly flow into the gap so that a sharp pressure peak and drastic pressure drop cannot be caused; (2) the centrifugal force generated by the vortex flow can lower the pressure inside the vortex chamber to some extent to form a sunken distribution which plays a role similar to adding

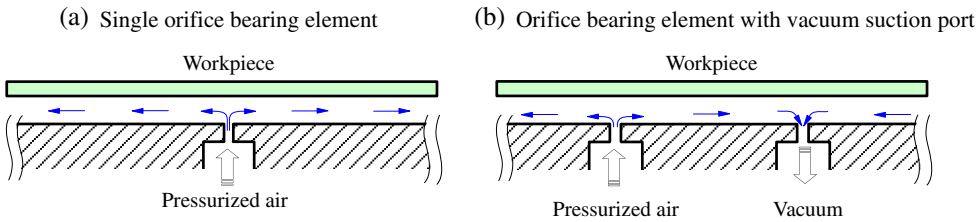

Fig. 2 Orifice bearing element. **a** Single orifice bearing element, **b** orifice bearing element with vacuum suction port

Fig. 3 Vortex bearing

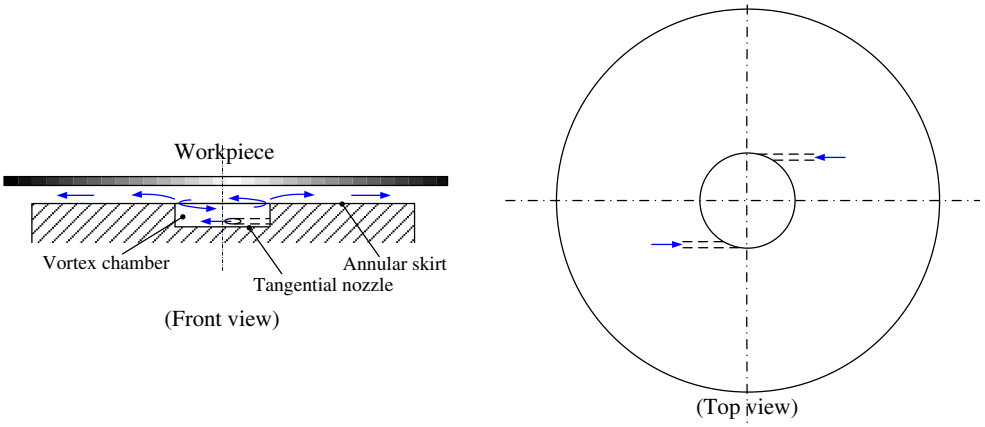

the vacuum suction port mentioned in Fig. 2b to narrow the clearance and increase the flotation stiffness [21–25]. Figure 4 shows an air conveyor for floating and transporting TFP glass substrates. The air conveyor consists of long rails on which the vortex bearing elements are embedded [7]. The array and size of vortex bearing elements are designed differently according to the requirement of flotation precision and air supply capacity etc. in actual applications.

Given that clarifying the basic characteristics of the new vortex bearing is very important for future optimization design and promoting practical applications, in this paper, we focus on one vortex bearing element to study its basic characteristics (flow rate characteristics, load capacity, and static stiffness) and flow phenomenon (pressure and velocity distributions), and we confirm its advantages in comparison to an orifice bearing. Figure 5 shows the vortex-bearing element used for experiments and discussion in this paper. It is made of aluminium and composed of several parts. First, a vortex ring with two tangential nozzles is glued to the body and a close board is glued to the vortex ring to form a vortex chamber. Then, a cover board is fixed to the body to form an air supply chamber. Therefore, compressed air can flow into the air supply chamber via the supply port and then get into the vortex chamber the two tangential nozzles. Figure 5b shows a photograph of the vortex bearing used in this study and Table 1 lists its main size parameters.

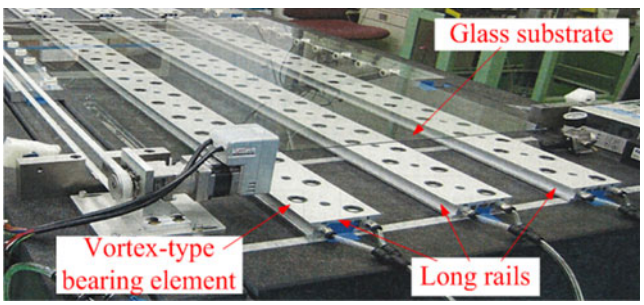

Fig. 4 Vortex-type air conveyor for transporting glass substrate [7]

3 Experimental setup and methods

For investigating the basic properties of the vortex bearing, we measure the pressure distribution and bearing force experimentally. The pressure distribution measurement not only shows the pressure distribution but also gives an insight into the flow phenomenon. The bearing force measurement evaluates the bearing force and flotation stiffness that indicate the most important properties of a bearing.

When conducting the experiments, the flow rate is fixed at a given constant value. In the case of large-scale air conveyors, a large number of bearing elements work simultaneously. Therefore, the flow rate of each bearing element is set as low as possible (usually several litres per minute (ANR)) to reduce the whole air consumption. Moreover, the floated workpiece (silicon wafer, TFP glass substrate) is relatively light. Therefore, in this study, the supply pressure and flow rate settings are less than 100.0 kPa (g) and 3.0 L/min (ANR) respectively, and the bearing force to be discussed is up to around 0.6 N.

3.1 Pressure distribution measurement

A sketch of the apparatus used to measure the pressure distribution is shown in Fig. 6. The test bearing can be fixed on the movable base and kept parallel to the stationary table by following the next steps. First, place the bearing on the stationary table and then adjust the three pins so that their tips touch the top of the bearing. Lock the pin clamps to hold the pins tightly and then release the spring. The spring pulls a string that is tied to both the bearing and the spring at its two ends to fix the bearing together with the movable base. The vertical position of the movable base is adjusted by turning a feeding bolt and measured through a dial meter with a resolution of 1 μm. This way, the clearance between the bearing and the stationary table becomes adjustable and measurable. A stationary table (Fig. 6b) is placed under the test bearing. A sliding bar containing a small tap hole and an internal connecting perforation is inserted through the middle of the stationary table. Such a design can also be seen in other's experimental work [26]. A

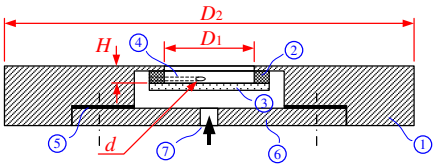

(a) Schematic diagram of the intersection of the test bearing element

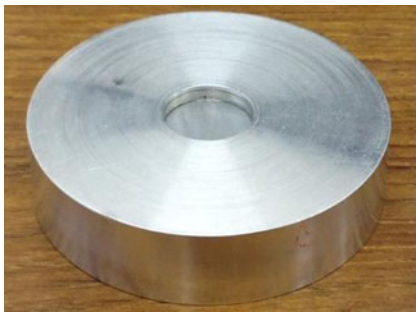

(b) Photograph of the test bearing element

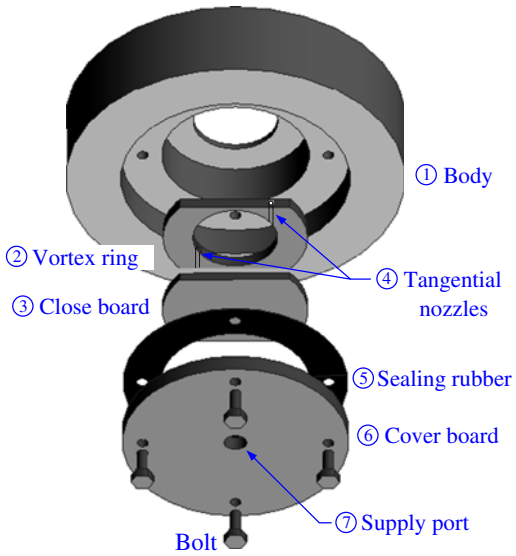

(c) Assembly schematic illustration

Fig. 5 Test vortex-type bearing element used in the study. **a** Schematic diagram of the intersection of the test bearing element, **b** photograph of the test bearing element, **c** assembly schematic illustration

wire-type position sensor is placed at one end of the bar to record its location. At the other end, a pressure sensor (PA-100, Copal Co., Ltd) is connected to the pressure tap to detect the pressure signal through the internal perforation. In this way, the pressure distribution on the upper surface of the stationary table can be measured by recording the pressure continuously while moving the sliding bar slowly. Comparing to the methods using limited pressure taps [27, 28], this method can present more details of pressure distribution.

3.2 Bearing force measurement

Figure 7 shows a sketch of the apparatus that is most used for measuring the relationship between the bearing force F and the clearance h [27, 29]. A plate is fixed on a shaft which is supported by an air guide (1X001-208, Oiles Co. Ltd) that has a high linear precision with less than ±3 μm deviation from the sliding direction; hence, the shaft and the plate can slide back and forth along the air guide with high parallel precision and no friction. The method used for the pressure distribution measurement is also used to fix the test bearing in parallel with the plate. A force sensor (LVS-200GA, Kyowa Co. Ltd.) placed on a slider lies on the other end of the shaft, and its front makes contact with the shaft. The back-and-forth position of the slider can be adjusted gradually by turning a feeding bolt, so that the force sensor, shaft, and plate can move to change the clearance h between the bearing and the plate.

Table 1 Size of the vortex bearing element (unit: mm)

H	d	D_1	D_2
3	0.3	15	60

Furthermore, the clearance change can be directly detected by a laser displacement meter (LC-2320, Keyence Co., Ltd).

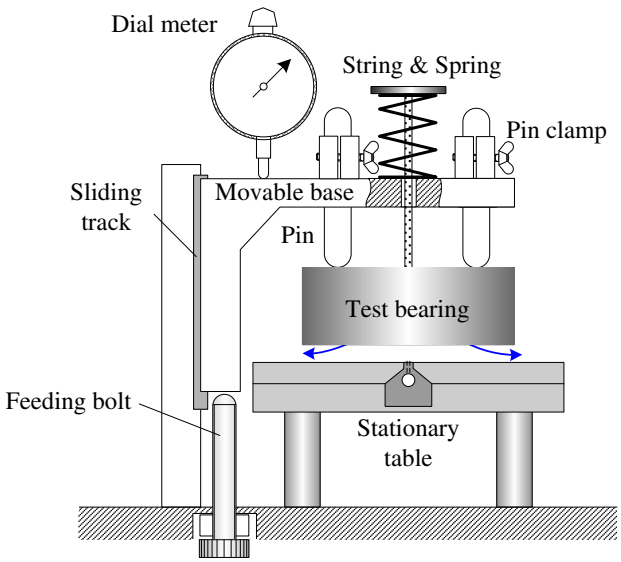

(a) Apparatus for pressure distribution measurement

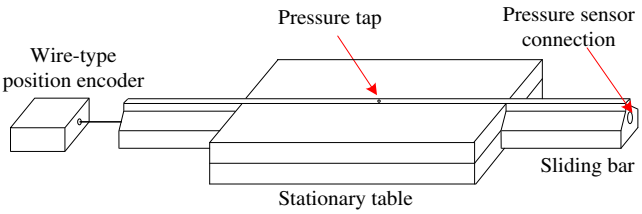

(b) Stationary table under the test bearing

Fig. 6 Apparatus for pressure distribution measurement. **a** Apparatus for pressure distribution measurement, **b** stationary table under the test bearing

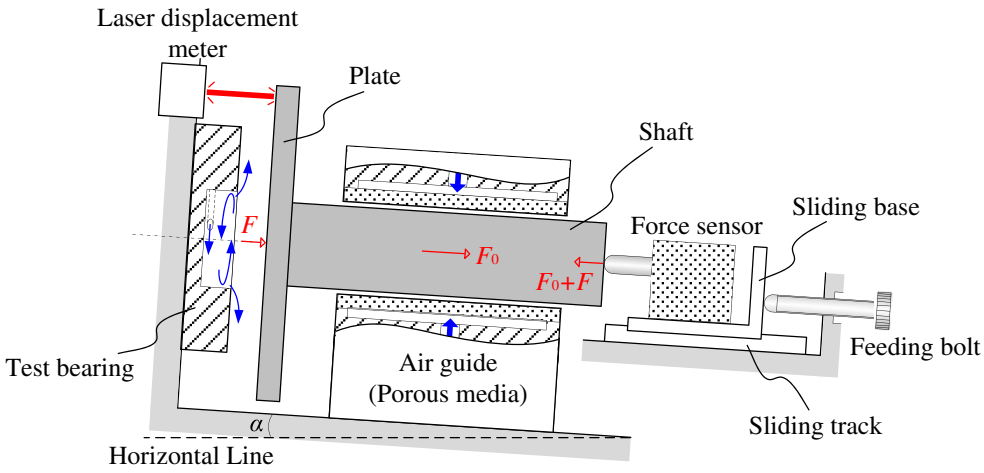

Fig. 7 Apparatus for bearing force measurement

Generally, the workpiece is placed upon the bearing. However, in order to facilitate the experimental operation, the entire apparatus is placed horizontally, as shown in Fig. 7. Air is light because of its small density, and thus, it is believed that placing the apparatus horizontally does not affect the experimental results. Moreover, the apparatus is in a slightly tilted position, and consequently, part of the gravity of the plate and the shaft, denoted by F_0, acts on the force sensor. After the air is supplied, the bearing applies a bearing force F to the plate that can be calculated by subtracting F_0 from the reading of the force sensor. By recording the clearance h simultaneously, the curve of load capacity (F–h) can be drawn.

3.3 Air supply circuit

The arrangement of the air supply circuit is shown in Fig. 8. Compressed air is supplied and regulated to a selected pressure. A thermal flow meter (FD-A10, Keyence Co. Ltd) and a pressure gauge are installed ahead of the test bearing to indicate the supply flow rate and upstream pressure.

4 Results and discussion

4.1 Flow rate characteristics

Two flow resistances exist in the vortex bearing: the tangential nozzles and the thin gap between the workpiece and the annular skirt. These two resistances determine flow rate characteristics of the vortex bearing, namely, the relationship between the supply pressure P_s and flow rate Q. Figure 9 shows the experimental P_s–Q curves when the clearance h is set to 0.08, 0.15, and 0.3 mm, respectively. The results reveal that the flow rate only changes with the pressure and is not affected by the clearance. In other words, the air resistance of the gap is far smaller than that of the tangential nozzles, which can be easily understood by comparing their flow area. The diameter of both tangential nozzles is 0.3 mm, so the total flow area is only 0.14 mm^2, while even the narrowest flow area of the gap is 2.4 mm^2, i.e., nearly 27 times bigger than the two nozzles. Therefore, the tangential nozzles dominate the flow rate characteristics of the bearing. In addition, it is shown in the next section that the pressure changes due to gap variation are only of 1–2 kPa. Such pressure changes have little impact on the flow rate characteristics of the nozzles. Therefore, we can consider the supply flow rate as constant once the supply pressure is set.

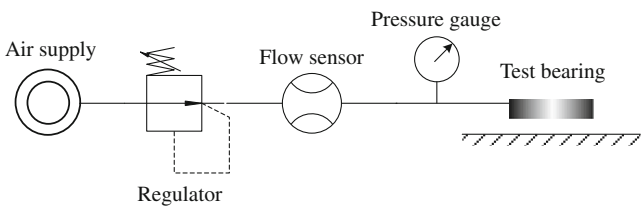

Fig. 8 Air supply circuit

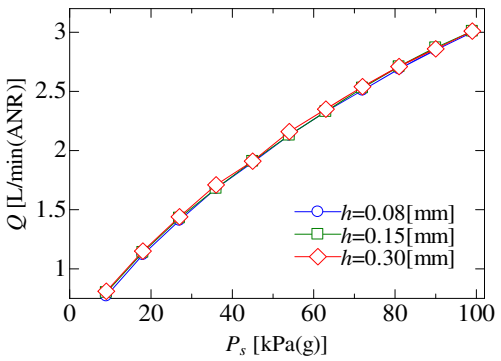

Fig. 9 Flow rate characteristics at different clearances

4.2 Pressure distribution

4.2.1 Pressure distribution of the vortex bearing

Two flow states with different properties exist in the vortex bearing: the vortex flow inside the vortex chamber and the gap flow in the gap. The vortex flow is dominated by fluid inertia (namely, centrifugal force), while the flow through the thin gap is mainly dependent on fluid viscosity. Generally, the flow state will be reflected by the pressure. Next, these two types of flow states as well as their interaction are investigated by trial measures of pressure distribution.

First, Fig. 10 shows the experimental result when Q is set to 2.0 and 3.0 L/min (ANR) and h is 0.15 mm. It can be seen that the pressure is distributed along the radial direction. Additionally, the vortex flow inside the vortex chamber ($r<D_1/2$) indicates a different distribution for the gap flow under the skirt ($D_2/2>r>D_1/2$). Inside the vortex chamber ($r<D_1/2$), the pressure at the central area is lower than at the periphery, for which the centrifugal force of vortex flow can well account. As illustrated in Section 2, the sunken pressure distribution at the centre can play to some extent a role similar to adding a vacuum suction port to drag the workpiece closer to the bearing. After air flows into the narrow gap ($D_2/2>r>D_1/2$) where viscous impedance becomes dominant, the pressure is distributed beyond the atmosphere and generally decreases along the air flow direction, which causes a supporting force to float the workpiece as the orifice bearing does.

Figure 10 also shows that the larger the supply flow rate, the faster the air blows from the nozzle; as a result, the pressure inside the vortex chamber sinks more significantly. On the other hand, a larger flow rate brings about more pressure loss because of the viscosity when flowing through the thin gap. Hence, it is observed that a higher pressure distribution is formed in the gap.

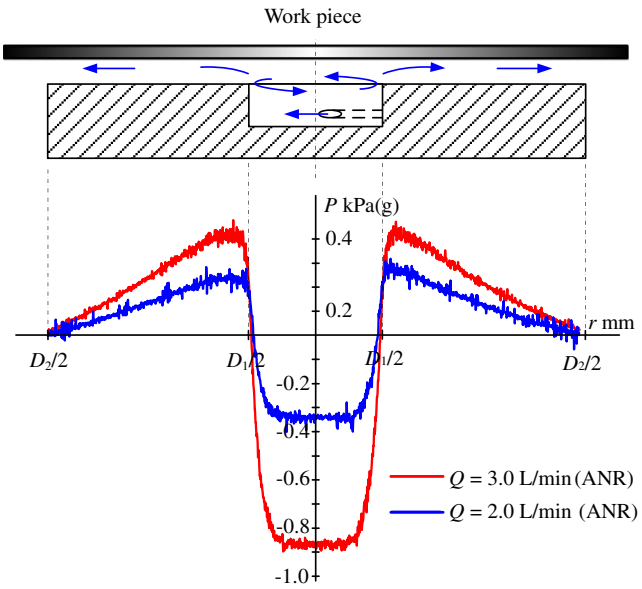

Fig. 10 Pressure distribution (h=0.15 mm, Q=2.0 L/min)

4.2.2 Vortex flow inside the vortex chamber

As to the unique vortex flow inside the vortex chamber, a further investigation of its velocity distribution is conducted. As is well known, pressure distribution reflects flow state. Given that the pressure distribution has been measured, the velocity and its distribution can be estimated by using the Navier–Stokes equation. Considering that the tangential velocity component, denoted by u_α, is dominant over other velocity components and the viscous effect in the case of the vortex flow, the Navier–Stokes equation can be written as follows [30]:

$$\frac{u_\alpha^2}{r} = \frac{1}{\rho}\cdot\frac{\partial P}{\partial r} \tag{1}$$

This indicates that u_α can be calculated by differentiating the pressure. Figure 11 shows the calculation results corresponding to the pressure distributions shown in Fig. 10. Note that air swirls with high speed around the periphery and the tangential velocity is distributed along the radial direction, while an obvious distribution cannot be observed in the central area. Increasing the supply flow rate would surely speed up the air swirling. We also know that the swirling velocity is far smaller than the speed when air is blown from the nozzle. Taking the case of Q=2.0 L/min (ANR) as an example, air is blown from the tangential nozzles with a mean velocity of ~235 m/s, and then, the flow slows down with the expansion

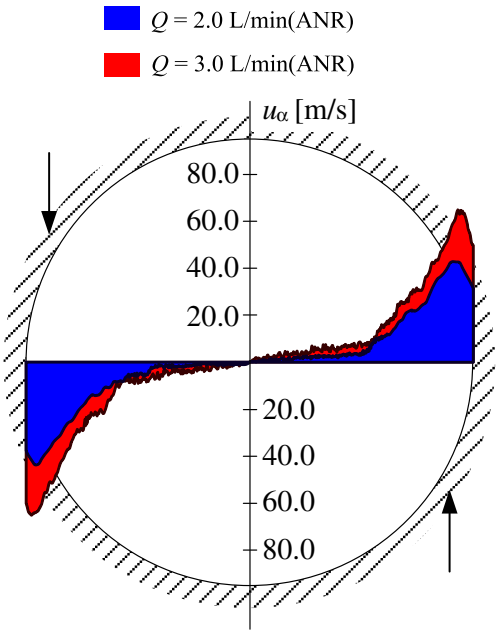

Fig. 11 Tangential velocity distributions (*black arrows* show the position of tangential nozzles)

of flow cross section so that even the peak of the distribution is only 1/5–1/6 of that at the nozzle outlet.

4.2.3 Comparison of vortex and orifice bearings

Figure 12 shows a comparison of pressure distribution between the orifice and vortex bearings at the same supply flow rate and clearance settings (Q=2.0 L/min (ANR), h=0.15 mm). The orifice bearing used for the experiments has the same structure as shown in Fig. 2a. The outside diameter is Φ60 mm, the same as the vortex bearing. Additionally, the diameter of the orifice is Φ0.55 mm, and thus, it has nearly the same flow rate characteristics as the vortex bearing. The comparison was conducted under the same supply flow rate. The supply flow rate is used as the experimental condition for the following reasons:

1. The supply flow rate is more suitable for indicating energy consumption, which is our target. Assuming that the conventional orifice and vortex bearings are supplied by the same air source (pump or blower), independently of how the requested pressure of air bearing is supplied, it is the same from the viewpoint of the air source because the air source provides the same pressurized air;
2. Usually, there are many other components in the air conveyors' supply system, e.g., long pipes, valves, elbows, and pressure regulators. When air is supplied through these components, energy loss certainly occurs and depends more on flow rate than on pressure. In terms of the whole system's energy consumption, the flow rate is important not only to the air bearings but also to its supply system.

First, the distribution curve of the orifice bearing shows that after the air emitting with high speed from the orifice directly impacts the workpiece, a very high pressure peak (up to nearly 50 kPa (g)) is formed; simultaneously, when air changes direction to flow into the gap, a prominent pressure drop occurs. Furthermore, because the air flowing radially through the gap shows an expected deceleration for small radius, the pressure displays a rising trend that is often designated as the Bernoulli effect. As the radius increases, the Bernoulli effect weakens and the viscosity in the thin gap gradually becomes dominant. Hence, the pressure then slowly decreases to the atmospheric pressure along the flow direction. Obviously, the pressure peak and the intense change at the central area would definitely bring about great concentrated stress acting on the workpiece, which are undesirable in the cases of floating and transporting fragile workpieces like thin glass substrates. In order to avoid this problem, the orifice conveyor usually has to decrease the supply pressure and simultaneously increase the number of bearings to gain enough flotation stiffness, which leads to excessive air consumption. In contrast, the vortex bearing solves the problem appropriately by setting the nozzles tangentially to obtain a much gentler pressure distribution.

4.2.4 Influence of the clearance

Next, we change the clearance to investigate how it influences the pressure distribution. Figure 13 shows the experimental results when the clearance h is set to 0.09, 0.10, 0.15, and 0.3 mm, respectively, and the supply flow rate is kept

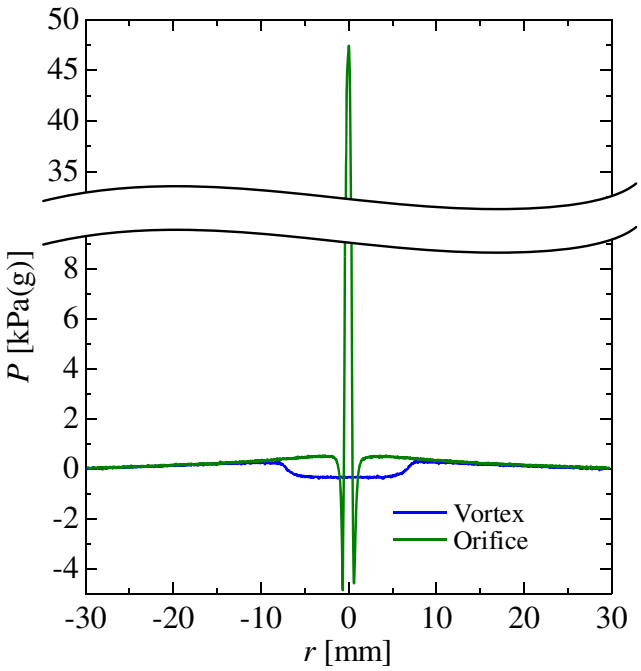

Fig. 12 Comparison of pressure distribution between vortex and orifice bearings (Q=2.0 L/min (ANR), h=0.15 mm)

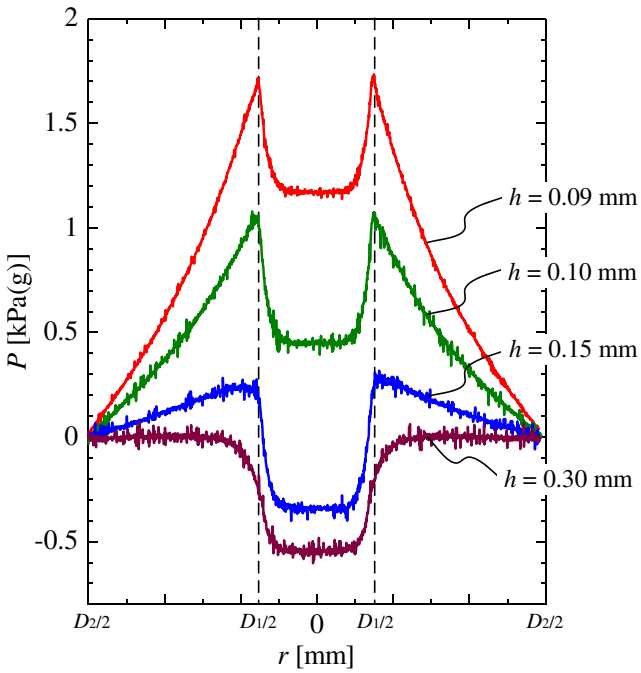

Fig. 13 Influence of clearance change (Q=2.0 L/min (ANR))

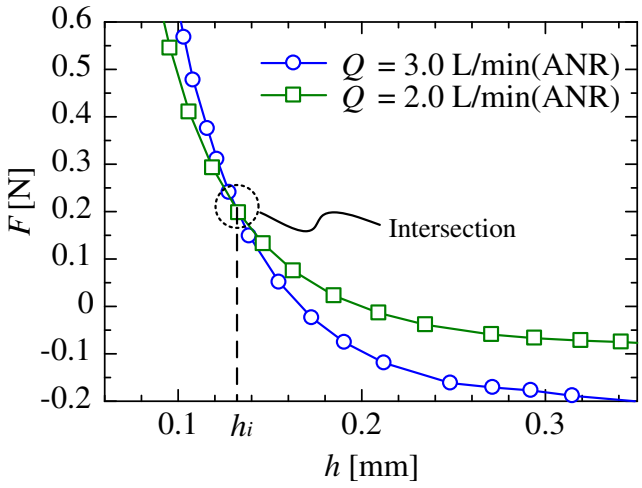

Fig. 14 Bearing force and clearance

constant. It can be observed that the distribution under the skirt ($D_2/2>r>D_1/2$) is very sensitive to the clearance change because it largely determines the viscous impedance of the gap. The larger the clearance, the weaker the viscous impedance, and therefore, the less significant the pressure distribution in the gap becomes. As a result, the pressure under the skirt almost equals the atmospheric pressure when the clearance is enlarged to 0.30 mm. On the other hand, the distribution inside the vortex chamber ($r<D_1/2$) roughly sustains a constant shape while fluctuating with the pressure change of the gap. Because the shape of the pressure distribution reflects the flow state, we can say that the vortex flow is hardly affected by the clearance change in the discussed clearance range.

4.3 Bearing force and stiffness

Using the experimental apparatus shown in Fig. 7, the load capacity, namely, the curve of the bearing force F and the clearance h, could be directly measured. Figure 14 shows the experimental results of the vortex bearing when the supply flow rate is set to 2.0 and 3.0 L/min (ANR). Note that the two curves of bearing force intersect each other. Defining the intersection clearance as h_i, when $h>h_i$, the larger the supply flow, the smaller is the bearing force; however, when $h<h_i$, the opposite tendency is observed. The unique flow structure of the vortex bearing can help us to understand this phenomenon. As mentioned above, the flow of the vortex bearing is mainly composed by the vortex flow (inertia flow) and the gap flow (viscosity flow). Which of the two flows is dominant decides how the force varies according to the supply flow rate. As can be confirmed in Fig. 13, in the case of smaller clearances ($h<h_i$), the pressure of the gap flow becomes much more significant than that of the vortex flow, that is, the gap flow prevails over the vortex flow. Therefore, when the clearance is constant, a larger supply flow rate gives rise to a bigger bearing force. However, as the clearance is enlarged to a certain extent, the viscous effect is weakened while the state of the vortex flow is hardly influenced by the clearance change so that it gradually surpasses the gap flow and becomes dominant. Consequently, in the case of larger clearances ($h>h_i$), the larger the supply flow rate, the stronger is the centrifugal force of the vortex flow, and therefore, the more sunken the pressure distribution of the central area, the weaker is the bearing force.

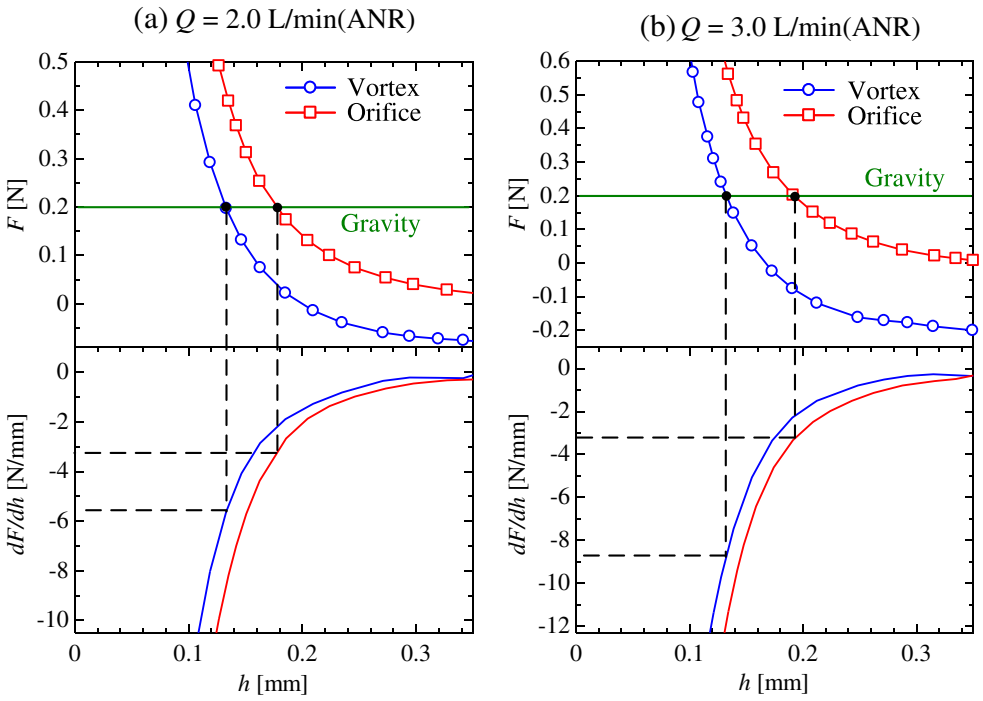

Fig. 15 Load capacity and stiffness. **a** Q=2.0 L/min (ANR) **b** Q=3.0 L/min (ANR)

Next, Fig. 15 shows the comparison between the vortex and the orifice bearings. The supply flow rate is set to 2.0 and 3.0 L/min (ANR), where the supply pressure is around 55.0 and 105.0 kPa (g), respectively. It is found that the bearing force of the vortex bearing is smaller than that of the orifice at the same clearance. It can be easily explained by the pressure distribution results shown in Fig. 12 that the vortex bearing has a sunken pressure distribution inside the vortex chamber while the orifice bearing produces a sharp pressure peak at the centre. Therefore, in general, the load capacity curve of the vortex bearing shifts down greatly from that of the orifice bearing. Concerning the static stiffness dF/dh, it can be calculated by differentiating the F–h curve. We notice that the static stiffness of the vortex bearing is a little smaller than that of the orifice bearing when the clearance is the same. As discussed in the last section, this can be explained by the fact that the clearance change hardly influences the flow state and shape of the resulting pressure distribution inside the vortex chamber. However, the pressure distribution of the orifice bearing at the central area is strongly influenced by the clearance changes. Hence, the results suggest that the clearance change affects the bearing force of the orifice bearing more than it does that of the vortex bearing.

Supposing that both of them float the same workpiece, for example, with a load gravity of 0.2 N, the curves of gravity and load capacity of the bearings intersect at two points. The workpiece is floated at the intersection points where the bearing force is equal to the gravity. Figure 15 shows that the vortex bearing floats the workpiece with a narrower clearance (about 40–60 μm narrower in this example) than the orifice. Furthermore, the corresponding flotation stiffness (absolute value) of the vortex bearing is also higher (more than twice in the case of Q=3.0 L/min (ANR)) than that of the orifice bearing. Such positive effects, which are usually achieved by having to add vacuum suction ports to orifice bearings, are realized by using vortex flow with a simple structure. In the case of an air conveyor floating glass substrates, one bearing unit is usually loaded from several grams to several tens of grams. Tables 2 and 3 show a comparison at various loads. The flotation stiffness of both bearings decreases as the load decreases. The ratio shows that the vortex bearing is superior to the orifice bearing, with more remarkable advantages when floating a lighter workpiece. As explained above, this is because a lighter load increases the clearance; hence, the vortex flow has a clear effect.

Table 2 Q=2.0 L/min (ANR) (P_s is around 55.0 kPa (g))

Load [N]		0.05	0.10	0.20	0.30
Stiffness [N/mm]	Vortex bearing	2.33	3.33	5.73	8.27
	Orifice bearing	0.67	1.40	3.20	5.47
	Ratio (Vortex : Orifice)	3.50	2.38	1.79	1.51

Table 3 Q=3.0 L/min (ANR) (P_s is around 105.0 kPa (g))

Load [N]		0.05	0.10	0.20	0.30
Stiffness [N/mm]	Vortex bearing	5.12	6.50	8.65	10.95
	Orifice bearing	1.00	1.70	3.25	5.15
	Ratio (Vortex : Orifice)	5.12	3.82	2.66	2.13

5 Conclusions and perspectives

In this paper, a new air-bearing element called as vortex bearing is introduced and studied. In comparison to the conventional orifice bearing, the new bearing is characterized by blowing air through tangential nozzles to form a vortex flow. The study focuses on one vortex-bearing element to investigate its basic characteristics (flow rate characteristics, pressure and velocity distributions, load capacity, and static stiffness). This study clearly shows that the vortex bearing takes advantage of vortex flow to form a sunken pressure distribution at the central area, so that it can apply a drag force to the workpiece to make it float closer to the bearing and therefore achieve higher flotation stiffness. Furthermore, blowing air tangentially instead of emitting directly onto the workpiece can avoid the formation of strong pressure distribution on the workpiece's surface, which would reduce the partial stress concentration acting on the workpiece. For these reasons, the new vortex bearing is applicable in air conveyors that float and transport workpieces such as TFP glass substrates and silicon wafers.

To promote the practical application of vortex bearing, the following issues will require further investigation in the near future:

1. While the workpiece floated on an air conveyor is passing through one bearing element, a variable bearing force would act on the workpiece's tip and therefore cause fluctuations in the workpiece's flotation. Air conveyors of vortex bearings have the same problem as those of conventional orifice bearings. It is necessary to study how fluctuations affect the flotation precision and find solutions to repress the undesirable fluctuation.
2. It is important to develop some theoretical or semi-empirical principles for the design of the vortex bearing.
3. The vortex bearing has a small vortex chamber at the centre which could cause an unstable phenomenon similar to a pneumatic hammer, as also happens to orifice bearings with a pocket space [15, 16]. Further investigation of this problem should be conducted.

Acknowledgments The authors thank Mr. Hideo Ozawa (Oiles Corporation) for his kind help and useful advice for the research. The authors gratefully acknowledge the financial support (no. 23760131) provided by the Japan Society for the Promotion of Science (JSPS).

Appendix 1: Uncertainty in the pressure distribution measurement experiment

In order to calculate the uncertainty in the pressure distribution measurement experiment (see Section 3.1), first we list the following factors that may cause measurement errors:

(1) The pressure sensor has been calibrated and the calibration uncertainty is estimated to be 0.1 % of the maximum reading. Given that the pressure sensor is analogue, the resolution is usually 0.1 % of the full range. Moreover, the analog noise signal has been experimentally confirmed as being around 35 Pa.

(2) The wire-type position encoder (digital) is used to record the position of the pressure value. The position error due to its calibration uncertainty and resolution affect the pressure measurement. Figure 10 shows that the intensively distributed region (e.g., around $r=D_1/2$) is very sensitive to the position error, while the sunken pressure distribution in the central region is hardly affected. Therefore, when converting the position error to pressure, the sensitivity coefficient is variable in a range of 0–680 Pa/mm, which can be calculated by differentiating the pressure versus position from the experimental pressure result of Fig. 10.

(3) The supply flow rate is set as the experimental condition and measured by the thermal flow rate sensor. The flow rate error due to the calibration uncertainty and resolution would affect the pressure measurement. According to the experimental result shown in Fig. 10, we know that increasing the supply flow rate from 2 to 3 L/min lowers the central pressure by 550 Pa. In addition, the pressure at $r=D_2/2$ is atmospheric and thereby does not change in spite of the flow rate change. Therefore, the sensitivity coefficient is variable in a range of 0–550 Pa/mm.

(4) The gap clearance is an experimental condition and measured by a dial meter. The gap clearance error, which is mainly caused by the calibration uncertainty and resolution of the dial meter, would affect the pressure measurement. Based on the experimental data of Fig. 13, we know that the 1-μm gap clearance change would lead to 70 Pa pressure change at the central region. However, there is little pressure change at $r=D_2/2$, where the pressure is atmospheric. Therefore, the sensitivity coefficient of the gap clearance error is variable in a range of 0–70 Pa/μm.

Because the measurement values are read and recorded by a computer, the error from reading and recording is disregarded. Further detailed information on the above possible error sources, e.g., specific values, probability distribution, and divisor, are listed in Table 4. Next, we convert these individual errors to the standard uncertainty in pascals and calculate the combined standard uncertainty by squaring the individual uncertainties, adding them, and then taking the square root of the total. Finally, we multiplied the result by a coverage factor (=2) to obtain the expanded uncertainty [31, 32].

The uncertainty of the pressure measurement is 40.0–74.8 Pa. This is based on the standard uncertainty multiplied by the coverage factor of 2, providing a level of confidence of approximately 95 %. Based on the above analysis, we also know that large uncertainty would be expected at

Table 4 Uncertainty in the pressure distribution measurement

Source of uncertainty	Value	Sensitivity coefficient	Converted value	Probability distribution	Divisor	Standard uncertainty
Calibration uncertainty of pressure sensor	1 Pa	1	1 Pa	Normal	2	0.5 Pa
Resolution of pressure sensor	1 Pa	1	1 Pa	Rectangular	$\sqrt{3}$	0.6 Pa
Noise of pressure sensor	35 Pa	1	35 Pa	Rectangular	$\sqrt{3}$	20.2 Pa
Calibration uncertainty of wire-type position sensor	0.06 mm	0–680 Pa/mm	0–40.5 Pa	Normal	2	0–20.25 Pa
Resolution of wire-type position sensor	0.02 mm	0–680 Pa/mm	0–13.5 Pa	Rectangular	$\sqrt{3}$	0–7.8 Pa
Calibration uncertainty of flow rate sensor	0.003 L/min	0–550 Pa/(L/min)	0–1.65 Pa	Normal	2	0–0.83 Pa
Resolution of flow rate sensor	0.01 L/min	0–550 Pa/(L/min)	0–5.5 Pa	Rectangular	$\sqrt{3}$	0–3.2 Pa
Calibration uncertainty of dial meter	0.3 μm	0–70 Pa/μm	0–21 Pa	Normal	2	0–10.5 Pa
Resolution of dial meter	0.5 μm	0–70 Pa/μm	0–35 Pa	Rectangular	$\sqrt{3}$	0–20 Pa
Combined standard uncertainty	–	–	–	Assumed normal	–	20.2–37.4 Pa
Expanded uncertainty	–	–	–	Assumed normal	2	40.0–74.8 Pa

Table 5 Uncertainty in the bearing force measurement

Source of uncertainty	Value	Sensitivity coefficient	Converted value	Probability distribution	Divisor	Standard uncertainty
Resolution of force sensor	2 mN	1	1 mN	Rectangular	$\sqrt{3}$	1.15 mN
Calibration uncertainty of force sensor	0.6 mN	1	0.6 mN	Normal	2	0.3 mN
Noise signal of force sensor	5 mN	1	5 mN	Rectangular	$\sqrt{3}$	2.89 mN
Resolution of laser displacement meter	0.1 μm	0–12.0 mN/μm	0–1.2 mN	Rectangular	$\sqrt{3}$	0–0.69 mN
Calibration uncertainty of laser displacement meter	0.4 μm	0–12.0 mN/μm	0–4.8 mN	Normal	2	0–2.4 mN
Noise signal of laser displacement meter	0.4 μm	0–12.0 mN/μm	0–4.8 mN	Rectangular	$\sqrt{3}$	0–2.77 mN
Resolution of flow rate sensor	0.01 L/min	0–0.125 N/(L/min)	0–1.25 mN	Rectangular	$\sqrt{3}$	0–0.72 mN
Calibration uncertainty of flow rate sensor	0.003 L/min	0–0.125 N/(L/min)	0–3.75 mN	Normal	2	0–1.88 mN
Friction of air guide	0 N	1	0 N	Rectangular	$\sqrt{3}$	0 N
Combined standard uncertainty	–	–	–	Assumed normal	–	3.12–5.27 mN
Expanded uncertainty	–	–	–	Assumed normal	2	6.24–10.54 mN

around $r=D_1/2$ where the pressure distribution is intensive, while small uncertainty would appear at the peripheral region where the pressure is close to atmospheric pressure.

Appendix 2: Uncertainty in the bearing force measurement experiment

In order to calculate the uncertainty of the bearing force measurement (see Section 3.2), first, we list the following factors that may cause measurement errors:

(1) The calibration uncertainty of the force sensor is estimated to be 0.1 % of the maximum reading. Given that the force sensor is analog, the resolution is usually 0.1 % of the full range. Moreover, the analog noise signal has been experimentally confirmed as being around 5 mN.
(2) A laser displacement meter is used to record the position of the force value. Its calibration uncertainty, resolution, and noise signal would cause errors of gap clearance. According to the stiffness data of Fig. 15, we can easily determine the sensitivity coefficient that is variable in a range of 0–12 mN/μm.
(3) As mentioned in Appendix 1, the flow rate sensor introduces a measurement error. Figure 14 shows that a flow rate change of 1 L/min would cause force changes of 0.125 N at the large clearance region. In addition, the bearing force is the same at the intersection position ($h=h_i$) despite the flow rate change. Therefore, the sensitivity coefficient is variable in a range of 0–0.125 N/(L/min).
(4) The plate and shaft used for force measurement are supported by the air guide so that we can disregard the effect of the friction force.

Because the measurement values are read and recorded by a computer, the error from reading and recording is disregarded. Further detailed information on the above possible error sources are listed in Table 5. Next, we convert these individual errors to the standard uncertainty in newtons and calculate the combined standard uncertainty by squaring the individual uncertainties, adding them, and then taking the square root of the total. Finally, we multiplied the result by a coverage factor (=2) to obtain the expanded uncertainty [31, 32].

The uncertainty of the bearing force measurement is 6.24–10.54 mN. It is based on the standard uncertainty multiplied by the coverage factor of 2, providing a level of confidence of approximately 95 %. Based on the above analysis, we also know that large uncertainty would be expected where the stiffness is high, while the measured force value of the region around $h=h_i$ would have small uncertainty.

References

1. Laurent GJ, Delettre A, Le FN (2011) A new aerodynamic-traction principle for handling products on an air cushion. IEEE Trans Robot 27:379–384
2. He X, Chen X (2007) The dynamic analysis of the gas lubricated stage in optical lithography. Int J Adv Manuf Technol 32:978–984
3. Paivanas JA, Hassan JK (1979) Air film system for handling semiconductor wafer. IBM J Res Develop 23(4):361–375
4. CoreFlow, www.coreflow.com/
5. New way air bearings, www.newwayairbearings.com/
6. Daiichi Institution Industry: http://www.daiichi-shisetsu.co.jp
7. Oiles corporation, http://www.oiles.co.jp/
8. Srinivas YL, Seetharamu KN, Parameswaran MA (1990) Investigation of air film conveyor pressurized through multiple holes. Finite Elem Anal Des 6:235–243

9. Lee HG, Lee DG (2006) Design of a large LCD panel handling air conveyor with minimum air consumption. Mech Mach Theory 41:790–806
10. Amano K, Yoshimoto S, Miyatake M (2011) Basic investigation of noncontact transportation system for large TFT-LCD glass sheet used in CCD inspection section. Precis Eng 35(1):58–64
11. Majumdar BC (1980) Externally pressurized gas bearings: a review. Wear 62:299–314
12. Gross WA (1963) Gas bearings: a survey. Wear 6:423–443
13. Devitt D (2009) The physics of glass flotation. Semicond Int Jpn 5:20–25
14. Stout KJ (1985) Design of aerostatic flat pad bearings using annular orifice restrictors. Tribol Int 18(4):209–214
15. Talukder HM, Stowell TB (2003) Pneumatic hammer in an externally pressurized orifice-compensated air journal bearing. Tribol Int 36(8):585–591
16. Ye YX, Chen XD, Hu YT, Luo X (2010) Effects of recess shapes on pneumatic hammering in aerostatic bearings. Proc Inst Mech Eng Part J-J Eng Tribol 224(3):231–237
17. Tomoo S, Shinichi T (1992) Improvement of the gas bearing stiffness by higher supply pressure (1st report). J Jpn Soc Precis Eng 58(4):621–627 (in Japanese)
18. Tomoo S, Shinichi T, Kunihiko U, Atsushi O (1992) Improvement of the gas bearing stiffness by higher supply pressure (2nd report). Journal of the Japan Society for Precision Engineering 58 (12):1995–2000 (in Japanese)
19. Ozawa, Kakuda, Yasuda (2010) "Noncontact air conveyor", Japan Patent, P2010-92724, April (in Japanese)
20. Li X, Horie M, Kagawa T (2011) 'An Experimental Investigation on Vortex Bearing'. Proceedings of 2011 International Conference on Fluid Power and Mechatronics 697–702
21. Li X, Kawashima K, Kagawa T (2011) Computational fluid dynamics study of a noncontact handling device using air-swirling flow. J Eng Mech–ASCE 137(6):400–409
22. Karagoz I, Kya F (2007) CFD investigation of the flow and heat transfer characteristics in a tangential inlet cyclone. Int Commun Heat Mass Transf 34:1119–1126
23. Cortes C, Gil A (2007) Modeling the gas and particle flow inside cyclone separators. Prog Energy Combust Sci 33:409–452
24. Li X, Kawashima K, Kagawa T (2008) Analysis on vortex levitation. Exp Therm Fluid Sci 32:1448–1454
25. Kumar R, Conover T (1993) Flow visualization studies of a swirling flow in a cylinder. Exp Therm Fluid Sci 7:254–262
26. Possamai FC, Ferreira RTS, Prata AT (2001) Pressure distribution in laminar radial flow through inclined disks. Int J Heat Fluid Flow 22:440–449
27. Paivanas JA, Hassan JK (1981) Attraction force characteristics engendered by bounded, radially diverging air flow. IBM J Res Develop 25(3):176–186
28. Ervin JS, Suryanarayana NV, Hon CN (1989) Radial, turbulent flow of a fluid between two coaxial disks. J Fluids Eng-Trans ASME 111:378–383
29. Wark CE, Foss JF (1984) Forces caused by the radial outflow between parallel disks. J Fluids Eng-Trans ASME 106:292–297
30. Currie IG (1993) Fundamental mechanics of fluids (2nd). McGraw-Hill
31. Bell S (2001) "A beginner's Guide to Uncertainty of Measurement". Good Measurement Practice Guide No.11, ISSN 1368-6550
32. Moffat RJ (1988) Describing the uncertainties in experimental results. Exp Therm Fluid Sci 1:3–17